



**HAL**  
open science

## Full exploration of the giant planet population around $\beta$ Pictoris

A. -M. Lagrange, M. Keppler, N. Meunier, J. Lannier, H. Beust, J. Milli, M. Bonnavita, M. Bonnefoy, S. Borgniet, G. Chauvin, et al.

### ► To cite this version:

A. -M. Lagrange, M. Keppler, N. Meunier, J. Lannier, H. Beust, et al.. Full exploration of the giant planet population around  $\beta$  Pictoris. *Astronomy & Astrophysics - A&A*, 2018, 612, <10.1051/0004-6361/201730436>. <insu-03693566>

**HAL Id: insu-03693566**

**<https://insu.hal.science/insu-03693566v1>**

Submitted on 13 Jun 2022

**HAL** is a multi-disciplinary open access archive for the deposit and dissemination of scientific research documents, whether they are published or not. The documents may come from teaching and research institutions in France or abroad, or from public or private research centers.

L'archive ouverte pluridisciplinaire **HAL**, est destinée au dépôt et à la diffusion de documents scientifiques de niveau recherche, publiés ou non, émanant des établissements d'enseignement et de recherche français ou étrangers, des laboratoires publics ou privés.



HAL Authorization

# Full exploration of the giant planet population around $\beta$ Pictoris $\star, \star\star$

A.-M. Lagrange<sup>1</sup>, M. Keppler<sup>1,2</sup>, N. Meunier<sup>1</sup>, J. Lannier<sup>1</sup>, H. Beust<sup>1</sup>, J. Milli<sup>3</sup>, M. Bonnavita<sup>4,5</sup>,  
M. Bonnefoy<sup>1</sup>, S. Borgniet<sup>1</sup>, G. Chauvin<sup>1</sup>, P. Delorme<sup>1</sup>, F. Galland<sup>1</sup>, D. Iglesias<sup>3,6</sup>, F. Kiefer<sup>7</sup>,  
S. Messina<sup>8</sup>, A. Vidal-Madjar<sup>7</sup>, and P. A. Wilson<sup>7</sup>

<sup>1</sup> Institut de Planétologie et d'Astrophysique de Grenoble, UMR5274 CNRS, Université Grenoble-Alpes, BP 53, 38041 Grenoble Cedex 9, France  
e-mail: [lagrange@obs.ujf-grenoble.fr](mailto:lagrange@obs.ujf-grenoble.fr)

<sup>2</sup> Max-Planck-Institut fuer Astronomie, Königstuhl 17, 69117 Heidelberg, Germany

<sup>3</sup> European Southern Observatory, Alonso de Cordova 3107, Vitacura, Santiago, Chile

<sup>4</sup> INAF – Osservatorio Astronomico di Padova, Vicolo dell'Osservatorio 5, 35122 Padova, Italy

<sup>5</sup> Institute for Astronomy, The University of Edinburgh, Royal Observatory, Blackford Hill, Edinburgh EH9 3HJ, UK

<sup>6</sup> Instituto de Física y Astronomía, Facultad de Ciencias, Universidad de Valparaíso, Av. Gran Bretaña 1111, 5030 Casilla, Valparaíso, Chile

<sup>7</sup> CNRS, UMR 7095, Institut d'Astrophysique de Paris, 98bis boulevard Arago, 75014 Paris, France

<sup>8</sup> Istituto Nazionale di AstroFisica, Osservatorio Astrofisico di Catania, Via S. Sofia 78, 95123 Catania, Italy

Received 13 January 2017 / Accepted 12 April 2017

## ABSTRACT

**Context.** The search for extrasolar planets has been limited so far to close orbit (typ.  $\leq 5$  au) planets around mature solar-type stars on the one hand, and to planets on wide orbits ( $\geq 10$  au) around young stars on the other hand. To get a better view of the full giant planet population, we have started a survey to search for giant planets around a sample of carefully selected young stars.

**Aims.** This paper aims at exploring the giant planet population around one of our targets,  $\beta$  Pictoris, over a wide range of separations. With a disk and a planet already known, the  $\beta$  Pictoris system is indeed a very precious system for studies of planetary formation and evolution, as well as of planet–disk interactions.

**Methods.** We analyse more than 2000 HARPS high-resolution spectra taken over 13 years as well as NaCo images recorded between 2003 and 2016. We combine these data to compute the detection probabilities of planets throughout the disk, from a fraction of au to a few dozen au.

**Results.** We exclude the presence of planets more massive than  $3 M_{\text{Jup}}$  closer than 1 au and further than 10 au, with a 90% probability.  $15+ M_{\text{Jup}}$  companions are excluded throughout the disk except between 3 and 5 au with a 90% probability. In this region, we exclude companions with masses larger than 18 (resp. 30)  $M_{\text{Jup}}$  with probabilities of 60 (resp. 90) %.

**Key words.** techniques: radial velocities – stars: individual:  $\beta$  Pictoris – techniques: high angular resolution – planets and satellites: detection

## 1. Introduction

$\beta$  Pictoris is one of the most exciting and studied young planetary systems identified among a growing sample. With its imaged debris disk of dust and giant planet, it is regarded as a precious proxy for the study of the early stages of planetary system formation and evolution, at a stage where giant planets are formed and most of the protoplanetary gas has disappeared from the disk. The  $\beta$  Pictoris system also allows us to study the interaction between planet(s) and disks. It has already been shown that  $\beta$  Pic b can explain several (but not all) of the dust disk characteristics; in particular its inner warp and some outer asymmetries (see Lagrange et al. 2010, 2012a).

There are hints of additional planets around  $\beta$  Pic. Thermal data have revealed blobs in the disk (Telesco et al. 2005; Okamoto et al. 2004; Wahhaj et al. 2003) that cannot be explained by only  $\beta$  Pictoris b. Also, ALMA observations revealed side asymmetries that could be due to the presence of other planets in the system (Dent et al. 2014). The relative void of material within  $\approx 50$  au of the star with respect to the 60–100 au region suggests that planets might be present within 50 au. Finally, the location of  $\beta$  Pictoris b on an inclined orbit could also be due to the gravitational perturbation by another planet. All this suggests (but does not prove) that additional planets may be present in the system. Searches for additional planets, either close to the star, using radial velocity techniques (Lagrange et al. 2012b), or further away, using direct high-contrast imaging, have been negative so far. Yet, the (mass, semimajor axis) space has not been fully explored due to lack of data.

In this paper, we aim at further exploring the  $\beta$  Pictoris environment using both types of data, and taking benefit from the use of several sets of data obtained over more

\* Based on data obtained with the ESO3.6 m/HARPS spectrograph at La Silla, and with NaCo on the VLT.

\*\* The RV data are only available at the CDS via anonymous ftp to [cdsarc.u-strasbg.fr](mailto:cdsarc.u-strasbg.fr) (130.79.128.5) or via <http://cdsarc.u-strasbg.fr/viz-bin/qcat?J/A+A/612/A108>

than 13 years. While the use of many sets of data is natural in the case of RV data (where timeseries are obtained), it was not realized until very recently that a single image is in general not enough to fully explore a planet population. In other words, the fact that we do not detect a companion with a given mass at a given projected separation in one image does not mean that we can rule out the presence of companions with such a mass orbiting at this separation. This is because, unless in the case of close to pole-on orbit orientations, planets can be at some phases too close to their stars in projected separations to be detected. Several sets of data, recorded at different epochs, are needed to fully explore the presence of planets and assess their detection probabilities. This effect is more important of course when considering planets with small semi major axis (sma), or when considering edge-on or close to edge-on systems (as in the case of  $\beta$  Pictoris). The paper is organized as follows: Section 2 briefly describes the data. Section 3 describes the estimation of the probability of planet detection for both RV and imaging data. Finally, we discuss in Sect. 4 the implication of these results on the  $\beta$  Pictoris system.

## 2. Observations and analysis

### 2.1. Radial-velocity data

More than 2110 high S/N spectra have been acquired with HARPS, between October 2003 and April 2016. Each spectrum contains 72 spectral orders, covering the spectral window 380–690 nm. The spectral resolution is approximately 110 000. The S/N of the spectra at 550 nm is varying between typically 150 and more than 400; it is about 300 on average. Most of the time, two consecutive few minutes-long individual spectra were recorded. Since March 2008, we recorded continuous 1–2 h long sequences of individual spectra in order to average out the large RV variations due to the stellar pulsations, which have periods in the range 20–30 min (see below). In the following, subset 2 refers to the data recorded in such long sequences. We refer to Lagrange et al. (2012b) for a more detailed description of  $\beta$  Pictoris HARPS data and variability characteristics.

Figure 1 shows the obtained RV time-series. Figure 2 gives examples of  $\approx 1.5$  h continuous monitorings of the RV. As already showed in Galland et al. (2006) and Lagrange et al. (2012a), periodic, high amplitude variations are observed, with periods of about 30 min. High-frequency photometric periodic variations have been reported as well (Koen 2003; Koen et al. 2003), with associated periods of 30–48 min and attributed to stellar pulsations, which led these authors to classify  $\beta$  Pictoris as a  $\delta$  Scuti star. Interestingly, these authors also analyzed a smaller set of spectroscopic data and found RV amplitudes of respectively  $129 \pm 27$ ,  $119 \pm 27$ , and  $30 \pm 27$  m/s for these three modes. Such values are roughly compatible with our observations if they refer to peak-to-peak values/2. In addition, we detect sometimes RV trends indicating variations on hour timescales that were not identified by Koen et al. (2003), as their data allowed them to look for high-frequency variations only (Koen, priv. comm.). Two examples are provided in Fig. 2. Examination of the night to night variations indicates that these variations, if periodic, have a period of less than one day.

### 2.2. Imaging data

$L'$ -band high-contrast images have been recorded with NaCo for slightly more than ten years: Nov. 10, 2003, Dec. 27, 2009, Sept. 17, 2010, Dec. 11, 2011, Oct. 12, 2011, Dec. 16, 2012,

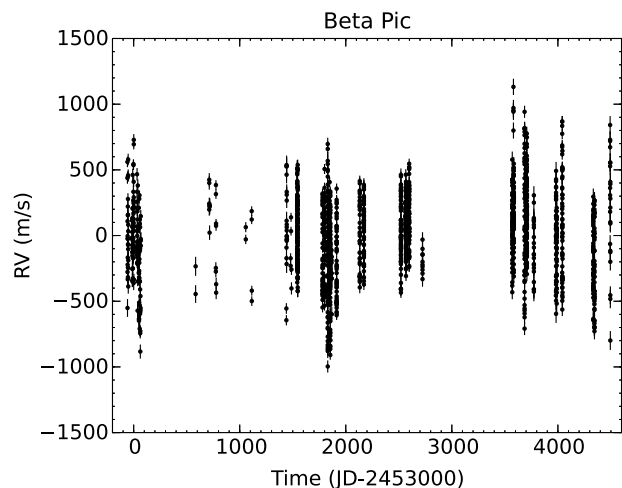


Fig. 1. Top: HARPS RV time-series of  $\beta$  Pictoris.

and Jan. 31, 2013. The pixel size is 27.1 mas ( $\approx 0.5$  au the  $\beta$  Pictoris distance), and typically, 1 full width at half maximum ( $FWHM$ ) = 3.6 px  $\approx 100$  mas. The first image was recorded in field-stabilized mode and is described together with its reduction procedure in Lagrange et al. (2009). It corresponds to the discovery image of the planet. The other images were obtained in Angular Differential Imaging mode (ADI); the last one was, in addition, obtained with the annular groove phase mask (AGPM; Absil et al. 2013); all these ADI data are extensively described (as well as the reduction procedures) in Milli et al. (2014). Pixel sizes and detector orientations were estimated using  $\Theta$  Ori C field for all data, as described in the aforementioned papers.  $5\sigma$  contrast maps were then estimated by measuring the noise over boxes of  $4 \times 4$  or  $64 \times 6$  pixels; these contrast maps were converted into detection limits in masses using BTSETTL models, and assuming an age of 21 Myr for the planets. In the case of ADI data, great care was devoted to estimating the ADI-induced self subtraction (see Milli et al. 2014).

## 3. Probability of the presence of planets

### 3.1. RV data

Planet presence probabilities (99% probability) were computed using the LPA method described in Meunier et al. (2012) and used Lagrange et al. (2012b). This method takes into account the temporal structure of the stellar noise and allows one to get improved detection limits in spite of the large stellar jitter (measured to be more than 300 m/s in the present dataset). The RV variations induced by the presence of  $\beta$  Pictoris b were not removed, as, with an estimated peak-to-peak amplitude of about 100 m/s over 3000 days, they contribute marginally to the overall variations. The detection limits obtained, assuming circular orbits as an illustration, and assuming a mass of 1.75 solar mass for the star, are shown in black in Fig. 3.

To possibly improve the detection limits, we tested two approaches. First, we fitted each continuous observing sequence of subset 2 with a sine function and determined the mean value of the sinusoidal fit over a period (see Fig. 2). The mean value represents the star's RV once corrected from the high-frequency pulsations. The detection limits obtained using these mean values (Fig. 3, blue curve) are slightly improved compared to the ones obtained when applying LPA on the raw RV data (black

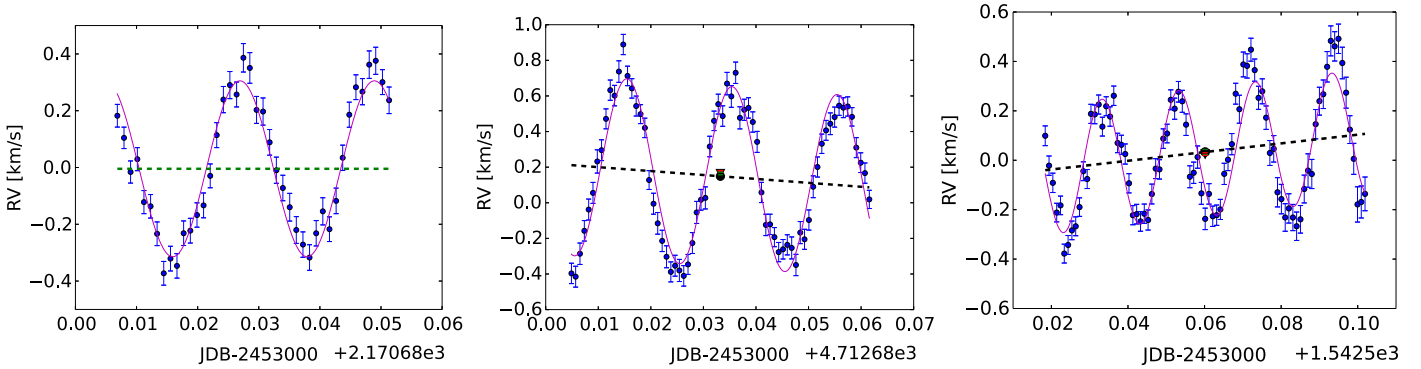


**Fig. 2.** Examples of fit of high frequency variations (pulsations) and average RV determination (see text). The data points are fitted by a sine function (continuous line) plus a slope (dashed line); the mean value over a period of the sine function gives the star RV corrected from the high-frequency pulsations. *From left to right:* example without drift, and two examples with drifts.

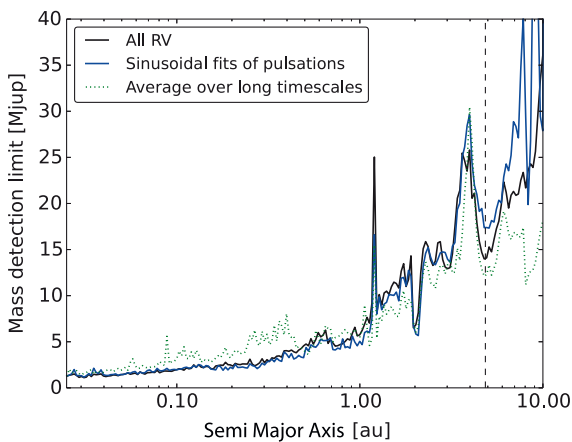


**Fig. 3.** Detection limits obtained taking as inputs all RV measurements, averaged RV and residual RV obtained after fitting the pulsations (see text), assuming circular orbits.

curve). As expected, this is not the case for larger sma, as subset 2 data span only eight years. Second, we averaged the data obtained between 2003 and 2016 over sequences of several days (typically 40 days), to get enough data points for each average. The obtained limits (Fig. 3, green curve) are slightly better than those obtained when applying LPA on the raw RV data for large sma.

Compared to previous work (Lagrange et al. 2012b), which used data recorded between October 2003 and February 2011 only, we note that the most recent data allow us to significantly increase the explored period range to  $P \approx 5000\text{--}6000$  days (up to 6 au). The detection limits are significantly improved especially for long period planets: for instance, in the 500–1000 days range, the detection limits were in the brown dwarf domain in this former paper, while they are now well within the planetary mass domain.

### 3.2. Imaging data

While the RV-derived detection limits can directly be interpreted in terms of probability to detect a planet with a given (mass, sma), the detection limits derived from imaging data have to be further processed to derive similar detection probabilities. Indeed, these detection limit maps give only the detection limits for a putative planet at a given position (PA, projected distance) from the star. This led Bonavita et al. (2012, see

also Bonavita et al. 2013) to develop a statistical tool based on a Bayesian approach, MESS, to estimate detection probabilities. Examples of use can be found in Rameau et al. (2013) or in Chauvin et al. (2015), for example. Recently, MESS2, an advanced version that takes into account imaging data from multiple epochs instead of only one, and can also handle imaging and RV data at the same time, was developed by Lannier et al. (2017). In practice, we generated 10 000 planets for each point in the (mass,sma) grid. The mass range explored in the grid was  $[0.5,80] M_{\text{Jup}}$ , at increments of  $0.4 M_{\text{Jup}}$ , and the sma range was  $[0.5,100]$  au, at increments of 0.5 au. We computed the positions of the generated planets at each observing period and checked whether the planet was detectable in at least one of the observing periods<sup>1</sup>.

We first used MESS2 with the imaging data only, and estimated the probabilities of presence of planets under three different assumptions on the planets’ orbital properties:

- all orbital parameters are free;
- the planets orbit within the dust disk with an inclination between 86 and 91 deg. This is justified by the fact that we look for planets within or close to the disk;
- the planets orbit within the dust disk with an inclination in the 86–91 deg range, and with an eccentricity  $e \leq 0.2$ . This constraint on the eccentricity is justified by the fact that we do not expect planets crossing  $\beta$  Pictoris b orbit. Hence, high eccentricity planets could be present with a limited range of semimajor axis only.

The resulting detection probability maps are given in Fig. 4. In each case, we overplot the iso-contours of detection probabilities considering values of 70, 80, 90, and 99%. The left part of each iso-contour has a classical shape given the obtained contrasts curves; the right, vertical part of the iso-contour at 90 and 99% in the top figure is due to the limitations imposed by the partial field of view (FoV) at large separations and for some inclinations, in the case of high eccentricity planets. This is expected as, for instance, planets with larger eccentricities have larger apelia, and can be outside the available FoV.

### 3.3. Combining RV and imaging data

Here, we consider both RV and imaging data. We generate, with MESS2, the same number of planets as before and we test whether the simulated planets are detected at least for one epoch

<sup>1</sup> Note that in 2010 and 2011, two epochs of observations separated by only two months were available; we combined the associated detection limits, so that we finally deal with five apparent epochs only.

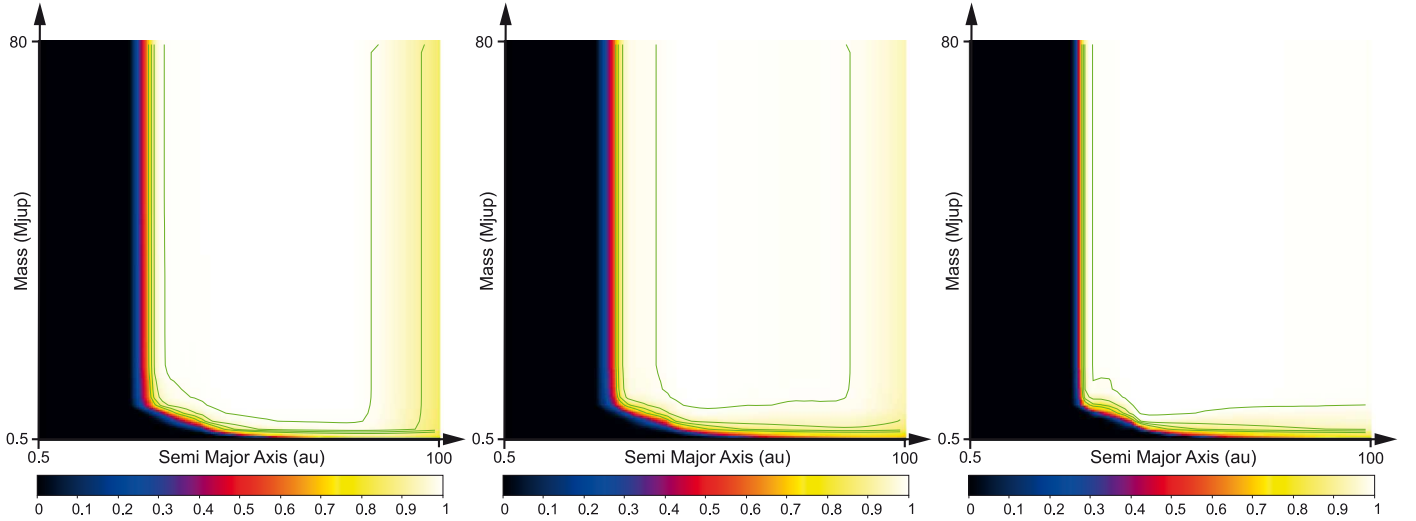


**Fig. 4.** Probability maps (sma, mass) derived using all NaCo imaging data. *From left to right:* (a) all orbital parameters are free; (b) the planets orbit in the dust disk with an inclination between 86 and 91 deg; (c) the planets orbit in the dust disk with an inclination in the 86–91 deg range, and with an eccentricity  $e \leq 0.2$ . The sma range from 0.5 to 100 au and the masses from 0.5 to 80  $M_{\text{Jup}}$ . The isocontours indicate probabilities of 0.7, 0.8, 0.9, and 0.99.

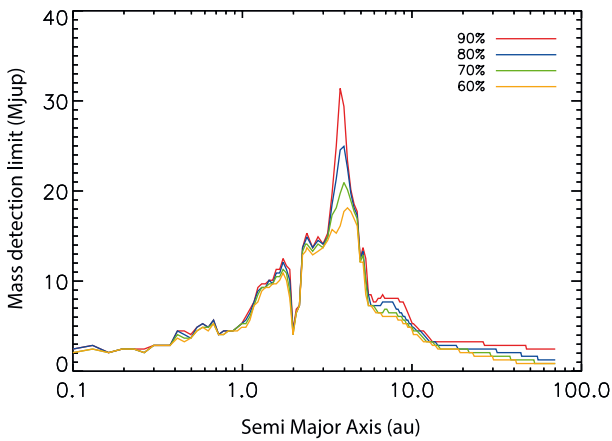


**Fig. 5.** 90 (red), 80 (blue), 70 (green), and 60 (orange) % detection probabilities using both the RV and imaging data ( $e \leq 0.2$  and  $i = 86\text{--}90$  deg).

in direct imaging or in RV. To know if a planet is detected in RV, we compute the RV series associated to each simulated planet at the time of observations and we test whether the planet is detectable or not by comparison with the observed RV time-series (see details in Lannier et al. 2017). Depending on the planet sma, we choose to use either the RV data curve derived from subset 2 only, or from the whole set of data (see above). The results are provided in Fig. 5.

#### 4. Additional giant planets around $\beta$ Pictoris

The present sets of RV and imaging data allow us, for the first time, to bridge the gap between long-period and short-period companions with zero or low eccentricities around  $\beta$  Pictoris. Except between 3 and 5 au, we can now rule out the presence of companions with masses larger than 14  $M_{\text{Jup}}$  with a 90% probability. The 3–5 au range remains less constrained: brown dwarfs with masses less than 18  $M_{\text{Jup}}$  (resp. 30  $M_{\text{Jup}}$ ) cannot be excluded with a probability of 60 (resp. 90) %. Planets more massive than 5  $M_{\text{Jup}}$  and sma smaller than 1 au or larger than

10 au can be excluded with a 90% probability. Hence, we conclude that the probability that  $\beta$  Pictoris hosts brown dwarfs or very massive planets in addition to  $\beta$  Pictoris b at various separations is low. The  $\beta$  Pictoris system therefore cannot resemble the HR8799 one.

##### 4.1. Giant planets to explain $\beta$ Pictoris b position above the main disk

The  $\beta$  Pictoris disk has long been observed as warped, with an inner part inclined by a few degrees with respect to the main outer disk. This very fact has been used to predict the presence of a BD or planet companion to  $\beta$  Pictoris (Mouillet et al. 1997; Augereau et al. 2001). Lagrange et al. (2012b) showed that indeed  $\beta$  Pictoris b is orbiting in a plane inclined above the main disk and is then most probably producing the disk warp. Yet, the mechanism responsible for  $\beta$  Pictoris b inclined orbit is still unknown. Answering this question is beyond the scope of our paper, but we wish to investigate how the present data may help to address the question. Some gravitational perturbation gave  $\beta$  Pic b its current inclination. The first scenario we can rule out is the perturbing action of a passing star. Indeed, in such a case, the flyby capable of tilting  $\beta$  Pic b would have had a much more dramatic action on the outer main disk structure that would clearly be visible today. The “perturber” was therefore within the disk. Depending on the exact mechanism at work, it may or may not still be in the disk. If the inclination is caused by regular secular perturbations between  $\beta$  Pic b and a planet of comparable mass or more massive, the perturber should still be there. The conclusion would be identical in the case of a more violent interaction with an inner massive planet, implying a past episode of large-scale instability if the  $\beta$  Pic system is comparable to the popular Nice model (Tsiganis et al. 2005). On the contrary, in the case of a close encounter between  $\beta$  Pic b and a not so massive planet, the planet could have been ejected.

In the case of a massive planet still in the disk, the present data show that the only range where another yet unseen planet of comparable mass could reside is between  $\sim 2$  and  $\sim 6$  au. In addition, if still present, the planet should have, through its own gravitational perturbation, impacted the disk inclination within a

radius roughly  $(M_b/M_c) \times (a_b/a_c)^2$  times smaller than the radius of the observed warp ( $M$  and “ $a$ ” refer to the mass and sma, respectively, “ $b$ ” refers to  $\beta$  Pic b and “ $c$ ” to  $\beta$  Pic c). For instance, in the case of a putative equal mass additional planet located at 4.5 au, the impact on the disk would be within about 20 au, and the disk in this region should be less tilted than outwards. However, both planets should presumably orbit in different planes, meaning that the effect on the disk warp could be more complex than expected.

#### 4.2. Giant planets to explain mid-IR blobs

Belts have been reported in mid-IR images of the  $\beta$  Pictoris disk at various separations: 6.4, 16, 32, 52 au by various authors (see above), as well as (yet to a lesser extent) at optical wavelengths (Golimowski et al. 2006). According to Freistetter et al. (2007), the planets’ masses responsible for the outer blobs should be about 0.2–0.6  $M_{\text{Jup}}$  and their sma about 25 and 45 au, but there is a lot of uncertainty on these estimations (the planet mass “estimated for”  $\beta$  Pic b, was, for example, 1–5  $M_{\text{Jup}}$  and its sma 11.5–12.5 au). Freistetter et al. (2007) has proposed the presence of at least three light (0.5–2  $M_{\text{Jup}}$ ),  $\approx$ zero eccentricity planets at 12, 24 and 44 au, to account for these gaps. Our present data allow us to rule out planets more massive than 1  $M_{\text{Jup}}$  at 44 au and about 1.5  $M_{\text{Jup}}$  at 24 au. So if present, such planets should have typical masses less than 1  $M_{\text{Jup}}$ .

#### 4.3. Giant planets to explain ALMA asymmetries

ALMA images revealed strong asymmetries in the NE/SW sides of the disk seen in continuum at 850  $\mu\text{m}$  with a brightness enhancement at 60 au (proj. separation) in the SW, as well as a prominent bulk of  $^{12}\text{CO}$  3–2 in the SW side of the disk, at a projected separation of  $\approx$ 85 au (Dent et al. 2014). Asymmetries are also detected in recent STIS data at optical wavelengths (Apai et al. 2015). Dent et al. (2014) propose that the CO bulk could be due to a physical clump. These features were tentatively explained by two alternative scenarios: a recent giant collision between two Mars-like planets, or by the migration of a few Earth-mass-planet-sweeping icy planetesimals into resonance. The planet would be currently close to the inner edge of the gas/dust belt ( $\approx$ 50–60 au), about 90 deg in front of the SW clump, and migrating outwards. New ALMA observations show a radial extension of the CO cloud favoring the second scenario (Matrà et al. 2017). Yet, our present data do not allow us to constrain the presence of such a light planet.

### 5. Concluding remarks and perspectives

We used RV and high-contrast images obtained between 2003 and 2013 (imaging) and 2016 (RV) to quantitatively constrain the presence of additional planets around  $\beta$  Pictoris to unprecedented limits. We can now bridge the gap between RV and imaging data, exploring then the full separation range from a fraction of one au to tens of au. We show that conversely to HR8799,  $\beta$  Pictoris is not surrounded by several massive planets.

The present analysis puts strong constraints on the putative planets possibly responsible for the blobs observed at mid-IR. New imaging data are needed to test sub-Jupiter-mass planets. This will be possible with the addition of new high-contrast data (new epochs), with NaCo and/or SPHERE. We note that, given the expected  $K_s-L'$  at 21 Myr, and given the respective

performances of SPHERE and NaCo, we do not expect SPHERE to be more sensitive than NaCo at large separations (e.g., 24 and 44 au). On the contrary, closer to the star, SPHERE will be far more sensitive than NaCo; for example a gain of 5–6 magnitudes is expected at 12 au, meaning that planets of  $\approx$ 1  $M_{\text{Jup}}$  should be detectable with SPHERE. We stress the fact that several years ( $\approx$ one decade) will be needed to acquire proper statistics on the probability of the presence of such planets around the star at such separations. Lighter planets will also be detectable at separations in the range 5–10 au. This is also true for the RV side: data acquired over longer time spans will improve the detection limits longwards of 2 au, and expand the accessible range to separations larger than 7 au. Finally, and very importantly, *Gaia* (Casertano et al. 2008) will allow us to dramatically improve the detection limits in the 0.5–4 au range. Combining RV, NaCo, SPHERE and *Gaia* data, the giant-planet population will be fully constrained.

These results are obtained even though  $\beta$  Pictoris is an unfavorable case for such a study: it has an intrinsic high stellar RV jitter, which limits the masses of detectable planets unless a very large number of spectra are acquired, and it is seen edge-on, which significantly decreases the efficiency of imaging (as putative planets spend significant amounts of time too close to the star to be detectable on a single image). Stars with intermediate inclinations can be explored with a much better efficiency (much less data needed), providing RV and imaging monitorings over long time spans. The first results from our dedicated HARPS and SPHERE/NaCo surveys will be presented in a forthcoming paper.

*Acknowledgements.* We acknowledge support from the French CNRS and the support from the Agence Nationale de la Recherche (ANR-14-CE33-0018), the OSUG LABEX. P.A.W. acknowledges the support of the French ANR, under program ANR-12-BS05-0012 “Exo-Atmos”. We thank M. F. Sterzik and G. LoCurto for performing some of the HARPS observations. AML thanks C. Koen and L. Balonas for discussions on the photometric and spectroscopic variations, and P. Rubini for his help on the developments of our RV measurement tool SAFIR. We finally thank the referee for his comments.

### References

- Absil, O., Milli, J., Mawet, D., et al. 2013, *A&A*, 559, L12  
 Apai, D., Schneider, G., Grady, C. A., et al. 2015, *ApJ*, 800, 136  
 Augereau, J. C., Nelson, R. P., Lagrange, A. M., Papaloizou, J. C. B., & Mouillet, D. 2001, *A&A*, 370, 447  
 Bonavita, M., Chauvin, G., Desidera, S., et al. 2012, *A&A*, 537, A67  
 Bonavita, M., de Mooij, E. J. W., & Jayawardhana, R. 2013, *PASP*, 125, 849  
 Casertano, S., Lattanzi, M. G., Sozzetti, A., et al. 2008, *A&A*, 482, 699  
 Chauvin, G., Vigan, A., Bonnefoy, M., et al. 2015, *A&A*, 573, A127  
 Dent, W. R. F., Wyatt, M. C., Roberge, A., et al. 2014, *Science*, 343, 1490  
 Freistetter, F., Krivov, A. V., & Löhne, T. 2007, *A&A*, 466, 389  
 Galland, F., Lagrange, A.-M., Udry, S., et al. 2006, *A&A*, 447, 355  
 Golimowski, D. A., Ardila, D. R., Krist, J. E., et al. 2006, *AJ*, 131, 3109  
 Koen, C. 2003, *MNRAS*, 341, 1385  
 Koen, C., Balona, L. A., Khadaroo, K., et al. 2003, *MNRAS*, 344, 1250  
 Lagrange, A.-M., Gratadour, D., Chauvin, G., et al. 2009, *A&A*, 493, L21  
 Lagrange, A.-M., Bonnefoy, M., Chauvin, G., et al. 2010, *Science*, 329, 57  
 Lagrange, A.-M., Boccaletti, A., Milli, J., et al. 2012a, *A&A*, 542, A40  
 Lagrange, A.-M., De Bondt, K., Meunier, N., et al. 2012b, *A&A*, 542, A18  
 Lannier, J., Lagrange, A. M., Bonavita, M., et al. 2017, *A&A*, 603, A54  
 Matrà, L., Dent, W. R. F., Wyatt, M. C., et al. 2017, *MNRAS*, 464, 1415  
 Meunier, N., Lagrange, A.-M., & De Bondt, K. 2012, *A&A*, 545, A87  
 Milli, J., Lagrange, A.-M., Mawet, D., et al. 2014, *A&A*, 566, A91  
 Mouillet, D., Larwood, J. D., Papaloizou, J. C. B., & Lagrange, A. M. 1997, *MNRAS*, 292, 896  
 Okamoto, Y. K., Katata, H., Honda, M., et al. 2004, *Nature*, 431, 660  
 Rameau, J., Chauvin, G., Lagrange, A.-M., et al. 2013, *A&A*, 553, A60  
 Telesco, C. M., Fisher, R. S., Wyatt, M. C., et al. 2005, *Nature*, 433, 133  
 Tsiganis, K., Gomes, R., Morbidelli, A., & Levison, H. F. 2005, *Nature*, 435, 459  
 Wahhaj, Z., Koerner, D. W., Ressler, M. E., et al. 2003, *ApJ*, 584, L27